Research on Chemical Intermediates (2024) 50:2581–2601
https://doi.org/10.1007/s11164-024-05281-x

Synthesis and characterization of solid Brønsted acid derived from rice husks as an efficient catalyst for the preparation of some 2,4,5-trisubstituted imidazole derivatives

Noor Abbas Alshook[1] · Hayder Hamied Mihsen[1] · Haitham Dalol Hanoon[1]

Received: 22 January 2024 / Accepted: 3 April 2024 / Published online: 25 April 2024

Abstract

Solid Brønsted acid catalysts are crucial heterogeneous catalysts used as substitutes for liquid Brønsted acids in organic synthesis. In this research, solid Brønsted acid was synthesised in an easy and environmentally friendly method using rice husks as a raw material by converting them to dissolved sodium silicate and using sol–gel technique, silylating agents ((3-chloropropyl)triethoxysilane (CPTES)) reacted with sodium silicate to prepare RH-SiO_2PrCl. Through the nucleophilic reaction between RH-SiO_2PrCl and 1-Amin-2-naphthol-4-sulfonic acid, a solid acid catalyst (RH-SiO_2PrANSA) was prepared. The solid acid catalyst is characterized by many techniques, such as FTIR, EDX, CHNS, and BET. The results showed a secondary amine absorption band (–N–H) at 3236 cm^{-1}. Also, the BET results for the catalyst indicated that its surface area was 61.74 m^2 g^{-1} with an average pore diameter of 5.14 nm. The synthesized solid Bronsted acid was used as a catalyst to prepare 2,4,5-Trisubstituted imidazole derivatives by reacting six different subtenant aldehydes with benzil and ammonium acetate. All the products are characterized by FTIR, H NMR, and Mass spectroscopy, with around ~ 90% conversion yields.

Keywords Rice husks · Solid Brønsted acid · Catalyst · Benzil · Imidazole derivatives

✉ Haitham Dalol Hanoon
alshebly1979@gmail.com

Hayder Hamied Mihsen
hayder.kandoh@uokerbala.edu.iq

[1] Chemistry Department, Collage of Science, University of Kerbala, Karbala, Iraq

Introduction

The increased amount of waste produced in manufacturing significantly impacts the environment, plants, and animals [1]. The recycling process is one of the solutions to reducing waste. The significance of using waste materials, such as rice husk (RH), has recently increased. RH refers to the outer layer of rice grains that is typically separated during milling. It is worth noting that this product constitutes around 20% of the global rice production [2]. According to FAO, the worldwide rice production in 2017 amounted to around 759.6 million tons. The husk consists of "cellulose (50%), lignin (25–30%), silica (15–20%), and moisture (10–15%)" [3, 4]. Interestingly, one of the sources of amorphous silica is rice husk extracted by sodium silicate. During a subsequent phase of the procedure, treating the sample with acid induces a transformation of the silica material into a gel substance. This extraction method could be conducted under ambient temperatures as a viable alternative to conventional heat treatment [5]. Solid acid catalysts have unique properties such as being environmentally friendly, easy to recycle, non-corrosive, and the catalyst can be reused for more than one catalytic cycle. Therefore, these solid acid catalysts have recently been used to produce biofuels [6–10]. A solid acid catalyst is produced safely through silica derived from rice husk. Solid materials with acidic characteristics on their surfaces can function as catalysts, similar to liquid acids like sulfuric acid and hydrochloric acid. Using solid acid catalysts enhances the efficiency and sustainability of chemical processes [11–13]. Heterocyclic compounds are the most extensive and varied group of organic chemicals. Aromatic heterocyclic compounds have been common structural patterns observed in various manufactured and naturally occurring bioactive, agrochemicals, and medicines [14]. Numerous studies have been conducted on using aromatic heterocyclic compounds as intermediates. Despite several efficient methodologies previously reported for synthesizing aromatic heterocyclic compounds and their derivatives, there is a continuous demand for the advancement of novel processes. One of the primary research endeavours in the synthesis field involves advancing novel synthetic methodologies for heterocyclic compounds. The objective is to enhance the molecular complexity level and the compatibility of functional groups in an atom-efficient and efficient manner. This is achieved by utilizing readily available starting compounds and conducting reactions under mild conditions [15]. Among the many nitrogen-containing heterocyclic compounds, imidazole is a central heterocyclic molecule prevalent in many bioactive compounds and synthetic drugs [16]. Hedyeh Hosseinzadeh etal. Reported short reaction times under a solvent-free condition to synthesize new imidazoles by efficient nano-catalyst. The nanocatalyst is produced from Hot-water-soluble starch (HWSS) material and nano-size conglomerates of talc and magnetite nanoparticles [17]. In the same context, magnetic silica nanoparticles were used in a simple and effective one-pot to synthesize imidazolate derivatives[18]. Suman Sangwan et al. reported an efficient approach for synthesising novel imidazoles with a reusable solid acid catalyst from rice husks [19]. Also, Nguyen et al. A new pathway

to synthesize polysubstituted imidazoles from nitro compounds was reported via the four-component condensation reaction in the presence of amorphous carbon-bearing sulfonic acid groups as solid acid catalysts [20]. Many methods synthesize imidazole derivatives, including a multicomponent response from a dicarbonyl, aldehyde, ammonia, or primary amine. These methods are used commercially to produce many imidazole derivatives under acidic conditions and at high temperatures. Still, these methods require long, hard work and expensive reagents. Therefore, we find safe and fast ways to produce heterogeneous acid catalysts using available and cheap raw materials. This catalyst can be used in multiple applications, including the production of imidazole derivatives [21, 22]. From this standpoint, our research aims to synthesise 2,4,5-trisubstituted imidazole derivatives in the context of solid Bronsted acid (SiO_2PrANSA) as a catalyst under mild conditions.

Materials and apparatus

The rice husks were taken from the Abbasiya factory in Najaf/ Iraq. All chemicals and solvents were purchased from Sigma-Aldrich®, TCI®, and Acros®. The FTIR analyses were recorded by Shimadzu 8400 s "Japan, with a spectral range from 4000 to 400 cm^{-1}. X-ray diffraction analyses were obtained by "Philips PW 1730/10" Using Cu-K radiation in an X-ray diffractometer. Elemental analyses (CHNS) were carried out on an Eager 300 for EA1112. Scanning electron microscopy (SEM-FESEM) was recorded by MIRA III (Czech). Atomic force microscopy (AFM) was obtained by (NT-MDT/INTEGRA (Holland), and Thermogravimetric analyses (TGA) were recorded by Apparatus SDT-Q600 concurrent TGA / DSC (Belgium) from 30 to 900 °C under nitrogen flow at a heating rate of 20 °C per minute. The NMR spectra were recorded using a Bruker 400 MHz NMR spectrometer from Germany. Mass spectroscopy was carried out by an Agilent 5375 d.

The preparation process of rice husks

The rice husk (RH) was collected from the quarry rice of Najaf, which was washed three times with distilled water and dried at room temperature for two days. 30 g of cleaned rice husk was stirred with 500 mL of 1 M nitric acid at room temperature for 24 h and washed many times very well and with distilled water until it reached pH 6–7 and dried in an oven at 110 °C overnight. The prepared sample was labelled as RH–NO_3.

Preparation of sodium silicate solution (RH-SiO_2) from rice husks

The preparation process of the non-crystalline sodium silicate from RH was performed using a recently reported method [23]; briefly, 30 g of RH-NO_3 were mixed with 200 mL of sodium hydroxide in a plastic container and stirred for 24 h. The mixture was filtered to remove the cellulose and then was dried. The filtered part

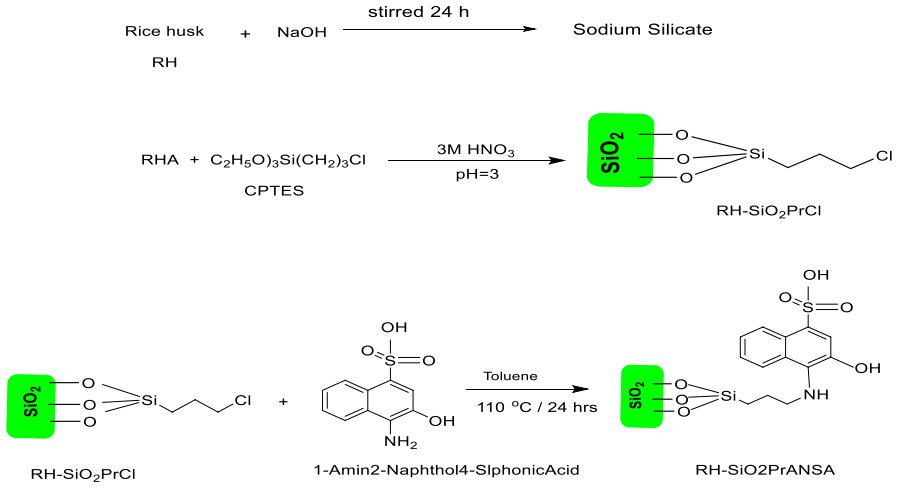

Scheme 1 Preparation process of sodium silicate, RH-SiO_2PrCl and RH-SiO_2PrANSA

represented sodium silicate and was used as a precursor to the synthesis catalyst, as shown in Scheme 1.

Preparation of rice husk silica-3-(chloropropyl) triethoxysilane (RH-SiO_2Pr Cl)

About 6 mL of (3-chloropropyl) triethoxysilane (CPTES) was added to 50 mL of the prepared sodium silicate solution. The mixture was titrated with 3 M HNO_3 until the pH reached 3. The formed gel was separated by centrifuge at 4000 r/min for 5 min. The mixture was washed with distilled water five times and finally washed with acetone, then dried up to 24 h at 110 °C in the oven. The prepared sample was labelled as RH-SiO_2PrCl, as shown in Scheme 1. The weight of the product was 6.4 g.

Preparation of acid catalyst (RH-SiO_2PrANSA)

A 0.5 g RH-SiO_2PrCl was added to (2 g, 8.3 mmol) of 1-Amin-2-naphthol-4-slphonic acid; the mixture was refluxed for 24 h at 80 °C in a mixture of 30 mL of toluene and (1.16 mL, 8.3 mmol) triethylamine (Et_3N). The resulting solution containing the yellow solid was filtered and washed with ethanol, acetone, and DMSO. Then dried for 24 h at 110 °C. Finally, 0.7 g of the powder was collected as RH-SiO_2PrANSA.

Synthesis 2,4,5-trisubstituted imidazole derivatives (4a-f)

A mixture of 5 mmol ammonium acetate, 1 mmol aldehyde and 1 mmol benzil was dissolved in 5 mL of ethanol, and then 0.08 g of RH-SiO_2PrANSA was added as a catalyst. The mixture was heated under reflux with stirring for 2.5 h. After

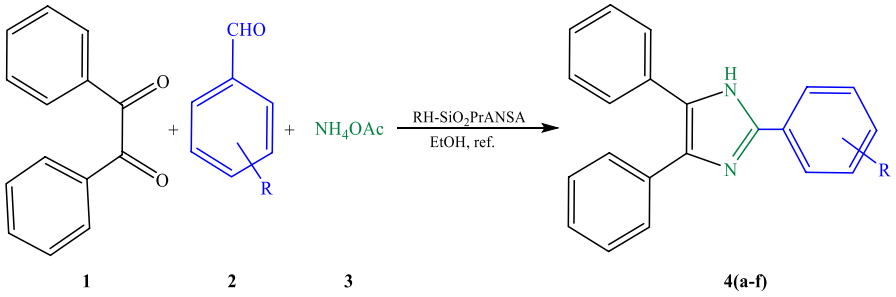

R = (a) H , (b) *p*-NO_2 , (c) *p*-$N(CH_3)_2$, (d) *m*-OH , (e) *p*-OH , (f) *p*-Cl

Scheme 2 Synthesis of some functional imidazole derivatives using RH-SiO2PrANSA as the catalyst

the reaction, the crude product was poured on dichloromethane (10 mL) with stirring for 15 min, and the solid Brønsted acid catalyst was removed by simple filtration. The catalyst was recovered in three successive cycles under the same conditions. The filtrate was poured into cold water (10 mL) and stirred for 10 min; a precipitated solid was filtered, washed with distilled water, and dried. The product was purified by recrystallizing it in an ethanol–water mixture to afford imidazole derivatives, as shown in Scheme 2. All the products were confirmed by melting points, FTIR, ^{1}H NMR and mass spectra.

2,4,5-triphenylimidazole (**4a**): Yield: 95%; beige solid; M.p. 271–273 °C (Lit. 271–273 °C) [24]; IR (KBr) $\bar{\upsilon}$ (cm^{-1}): 3317 (NH), 3063 (Ar–H), 1662 (C=N); ^{1}H NMR (400 MHz, DMSO-d_6) δ (ppm): 12.79 (s, NH), 8.10 (d, $J = 8.0$ Hz, 2H, Ar–H), 7.57–7.21 (m, 13H, Ar–H); MS (ESI): m/z = 296.3 [M^+].

2-(4-nitrophenyl)-4,5-diphenylimidazole (**4b**): Yield: 83%; yellow solid; M.p. 194–196 °C (Lit. 199–201 °C) [13]; IR (KBr) $\bar{\upsilon}$ (cm^{-1}): 3375 (NH), 3059 (Ar–H), 1600 (C=N), 1516 and 1338 (NO_2); ^{1}H NMR (400 MHz, DMSO-d_6) δ (ppm): 13.16 (s, NH), 8.37–8.33 (m, 3H, Ar–H), 8.32–7.26 (m, 11H, Ar–H); MS (ESI): m/z = 341.3 [M^+].

4-(4,5-diphenylimidazol-2-yl)-N,N-dimethylaniline (**4c**): Yield: 71%; beige solid; M.p. 259–261 °C (Lit. 256–258 °C) [25]; 3375 (NH), 3036 (Ar–H), 2939, 2877 and 2800 (C–H), 1612(C=N); ^{1}H NMR (400 MHz, DMSO-d_6) δ (ppm): 12.32 (s, NH), 7.92–7.89 (m, 2H, Ar–H), 7.51–7.30 (m, 10H, Ar–H), 6.81–6.78 (m, 2H, Ar–H), 2.97 (s, 6H, $N(CH_3)_2$); MS (ESI): m/z = 339.2 [M^+].

3-(4,5-diphenylimidazol-2-yl)phenol (**4d**): Yield: 97%; gray solid; M.p. 255–258 °C (Lit. 254–257 °C) [25]; IR (KBr) $\bar{\upsilon}$ (cm^{-1}): 3313 (OH), 3185 (NH), 3063 (Ar–H), 1662(C=N); ^{1}H NMR (400 MHz, DMSO-d_6) δ (ppm): 12.61 (s, NH), 9.56 (s, OH), 7.55–7.20 (m, 12H, Ar–H), 6.79–6.77 (m, 2H, Ar–H); MS (ESI): m/z = 312.1 [M^+].

4-(4,5-diphenyl-1H-imidazol-2-yl)-phenol (**4e**): Yield: 80%; gray solid; M.p. 236–238 °C (Lit. 233–236 °C) [25]; IR (KBr) $\bar{\upsilon}$ (cm^{-1}): 3313 (OH), 3167 (NH), 3063 (Ar–H), 1666(C=N); ^{1}H NMR (400 MHz, DMSO-d_6) δ (ppm): 12.41

(s, NH), 9.70 (s, OH), 7.91–7.88 (m, 2H, Ar–H), 7.54–7.19 (m, 10H, Ar–H), 6.87–6.83 (m, 2H, Ar–H); MS (ESI): m/z = 312.3 [M^+].

2-(4-chlorophenyl)-4,5-diphenylimidazole (**4f**): Yield: 95%; white solid; M.p. 263–265 °C (Lit. 260–262 °C) [25]; IR (KBr) $\bar{\upsilon}$ (cm^{-1}): 3437 (NH), 3066 (Ar–H), 1600 (C=N); ^{1}H NMR (400 MHz, DMSO-d_6) δ (ppm): 12.79 (s, NH), 8.10 (d, *J* = 8.0 Hz, 2H, Ar–H), 7.57–7.52 (m, 9H, Ar–H), 7.50–7.32 (m, 2H, Ar–H), 7.31–7.21 (m, 1H, Ar–H); MS (ESI): m/z = 330.3 [M^+].

Results and discussion

Fourier-transform infrared spectroscopic analysis (FT-IR)

The existence of a band within the range of 3600–3300 cm^{-1} in the FT-IR spectra of RH-SiO_2PrCl, as seen in Fig. 1, the occurrence of a stretching vibration associated with the hydroxyl group in Si–OH and adsorbed water on the silica surface [26]. The prominent peak observed at 2950 cm^{-1} can be attributed to the stretching vibration modes associated with the C–H bonds [4]. A band at 1639 cm^{-1} may be attributed to the bending vibration of water molecules [27]. The FT-IR examination of the RH-SiO_2PrCl sample revealed the presence of distinct bands with peaks at 1087, 790, and 495 cm^{-1}. These bands correspond to the vibrational modes associated with the siloxane (Si–O–Si) bonds [12]. A band at 690 cm^{-1} suggests that this can be attributed to the carbon chloro bond in the RH-SiO_2PrCl. The findings of this study provide unequivocal evidence of the effective integration of CPTES into sodium silicate.The spectum on the new catalyst RH-SiO_2PrANSA showed a broad band around 3445 cm^{-1} due to silanol groups (Si–OH) and to the absorption frequency of water adsorbed on the silica surface. Also, the FT-IR study conducted on the new catalyst, as seen in Fig. 1, revealed the presence of a broad band at 3236 cm^{-1}. This band can be attributed

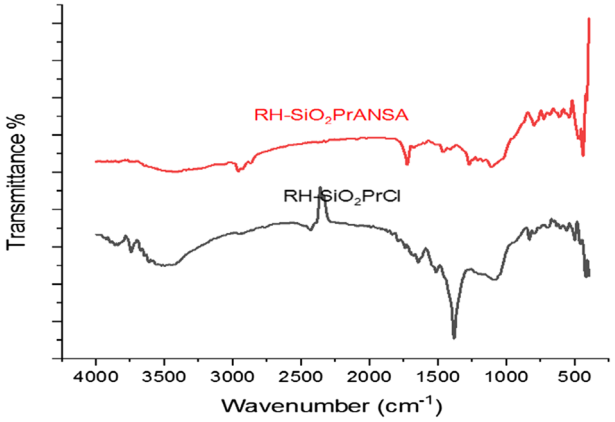

Fig. 1 FTIR analysis of RH-SiO_2PrCl and RH-SiO_2PrANSA

to the stretching vibration of the N–H group [4, 28], the presence of a band at 2966 cm^{-1} due to the C–H group stretching vibration. The band at 1400 cm^{-1} was attributed to the vibration of the extension of the S=O group due to the presence of sulfonic acid. Furthermore, the peak was observed around 1670 cm^{-1}, which is typically allocated to the vibration of adsorbed water (H_2O), and the peak located at 1095 cm^{-1} was assigned to Si–O–Si vibration [29]. All these absorption bands were successfully inducted to lade functionalized silica RH-SiO_2PrCl with 1-Amin-2-naphthol-4-sulfonic acid.

X-ray diffraction analysis (XRD)

The XRD patterns at low-angle and high angle of the functionalized silica RH-SiO_2PrCl and RH-SiO_2PrANSA are shown in Figs. 2, 3, respectively. From observing the XRD patterns at low angles, no changes were observed in the scattering angles, and thus, it is impossible to know the shapes of the pores and phases through XRD patterns at low angles. At a high angle, the first broad peak around 22° of 2 theta indicates the amorphous nature of RH-SiO_2PrCl and RH-SiO_2PrANSA [30, 31]. However, no change in the catalyst phase after adding the 1-Amin-2-naphthol-4-sulfonic acid immobilized onto RH-SiO_2-PrCl.

Nitrogen adsorption analysis

The N_2 adsorption–desorption investigation yielded findings indicating that the RH-SiO_2PrCl compound had a specific surface area value of 205.42 m^2 g^{-1} and a pore width of 3.97 nm, as seen in Fig. 4a and based on the IUPAC classification, the adsorption–desorption isotherm exhibits a type IV behavior [32], accompanied with hysteresis loops of H_2 nature. This observation suggests the presence of robust and attractive interactions among the molecules [33]. The specific surface area and

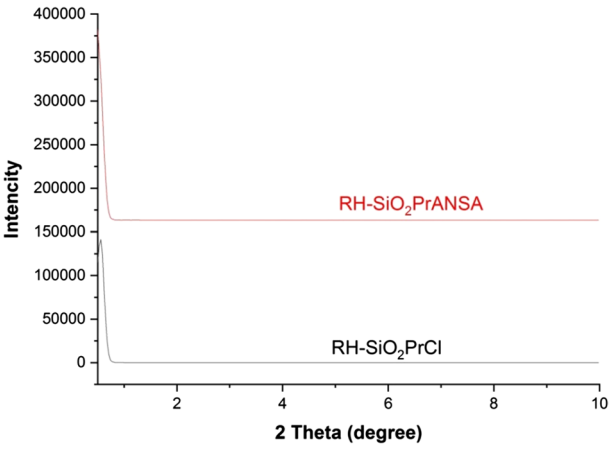

Fig.2 XRD analysis at low angle of RH-SiO_2PrCl and RH-SiO_2PrANSA

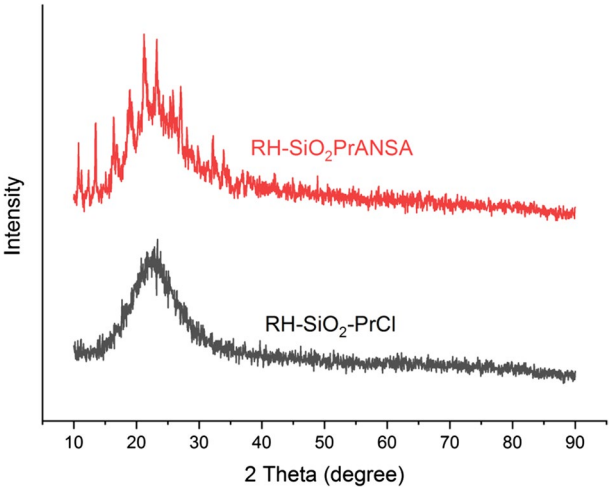

Fig.3 XRD analysis at high angl of RH-SiO_2PrCl and RH-SiO_2PrANSA

pore diameter of the RH-SiO_2PrANS were determined by BET analysis, as shown in Fig. 4b. The obtained values were 61.739 m^2 g^{-1} for specific surface area and 5.14 nm for pore diameter. The observed isotherms displayed a characteristic type IV curve, whereas the hysteresis loop was classified as type H_2 based on the IUPAC classification. It was observed that the decrease in the value of the specific surface area of the catalyst RH-SiO_2PrANS due to the replacement of 1-amino-2-naphthol-4-sulfonic acid with a chloro leads to cracking of the surface, which is crowded with the ligand network on the surface and thus clogs the tiny pores.

Thermogravimetric analysis (TGA)

Thermogravimetric analysis (TGA) was used to ascertain the thermal stability of RH-SiO2PrCl and RH-SiO_2PrANS. The TGA thermogram of RH-SiO_2PrCl, Fig. 5a, shows two distinct phases in the first phase, at a temperature ranging from 50 to 200 °C, attributed to loss of water adsorbed on the compound sample surface (about 10%). In the second stage, at a temperature from 200 to 850 °C, the weight loss increased by 37% because of the degradation of the chloropropyl groups attached to silica and the intensification of silanol groups to form the stable Si–O–Si siloxane bonds [34]. Thermogravimetric analysis (TGA) was used to ascertain the thermal stability of the catalyst RH-SiO_2PrANS. The TGA thermogram (Fig. 5b) shows two distinct phases in the first phase, at a temperature ranging from 50 to 200 °C, attributed to the water loss adsorbed on the compound sample surface (about 18%). Decomposition of the 1-Amin-2-naphthol-4-sulfonic acid bonded to the silica accounts (about 60%) for the second mass loss at a temperature from 200 to 650 °C. At high temperatures between 650 and 900 °C, the Si–OH groups break

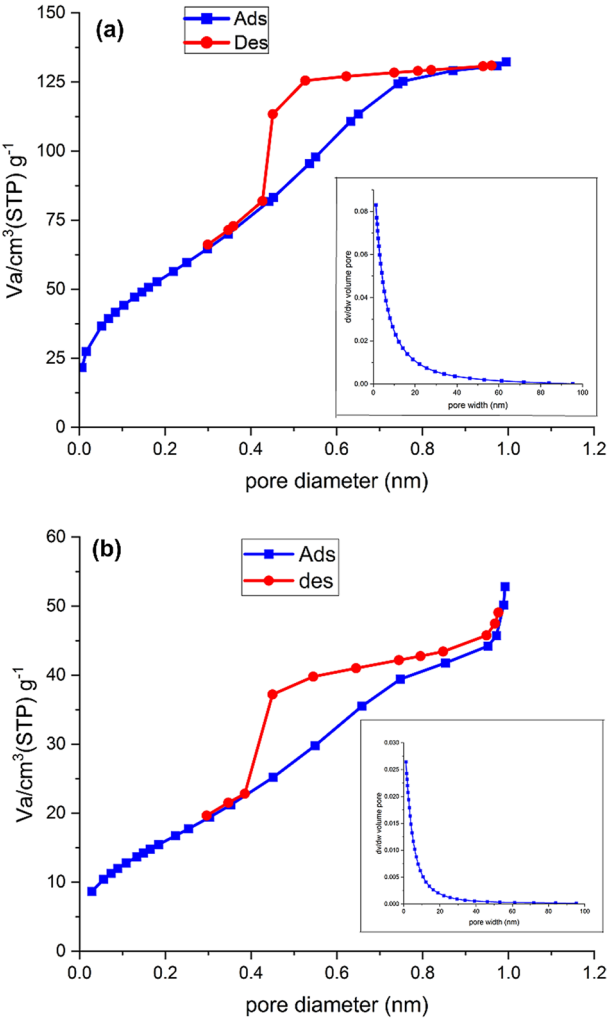

Fig. 4 **a** N_2 adsorption–desorption isotherm and pore size distribution of RH-SiO_2PrCl. **b** N_2 adsorption–desorption isotherm and pore size distribution of RH-SiO_2PrANS

down in the silica structure and transform into the Si–O–Si siloxane group (about 20%) [35, 36]

Elemental analysis (CHNS)

The elemental analysis (CHNS) of the RH-SiO_2PrCl compound showed that the percentage of carbon and hydrogen reached 16.24% and 5.3%, respectively. As shown in Table 1, the elemental analysis of the RH-SiO_2PrANSA compound exhibited that the percentage of carbon, hydrogen, nitrogen and sulfur was 29.41%, 7.3%, 3.5%

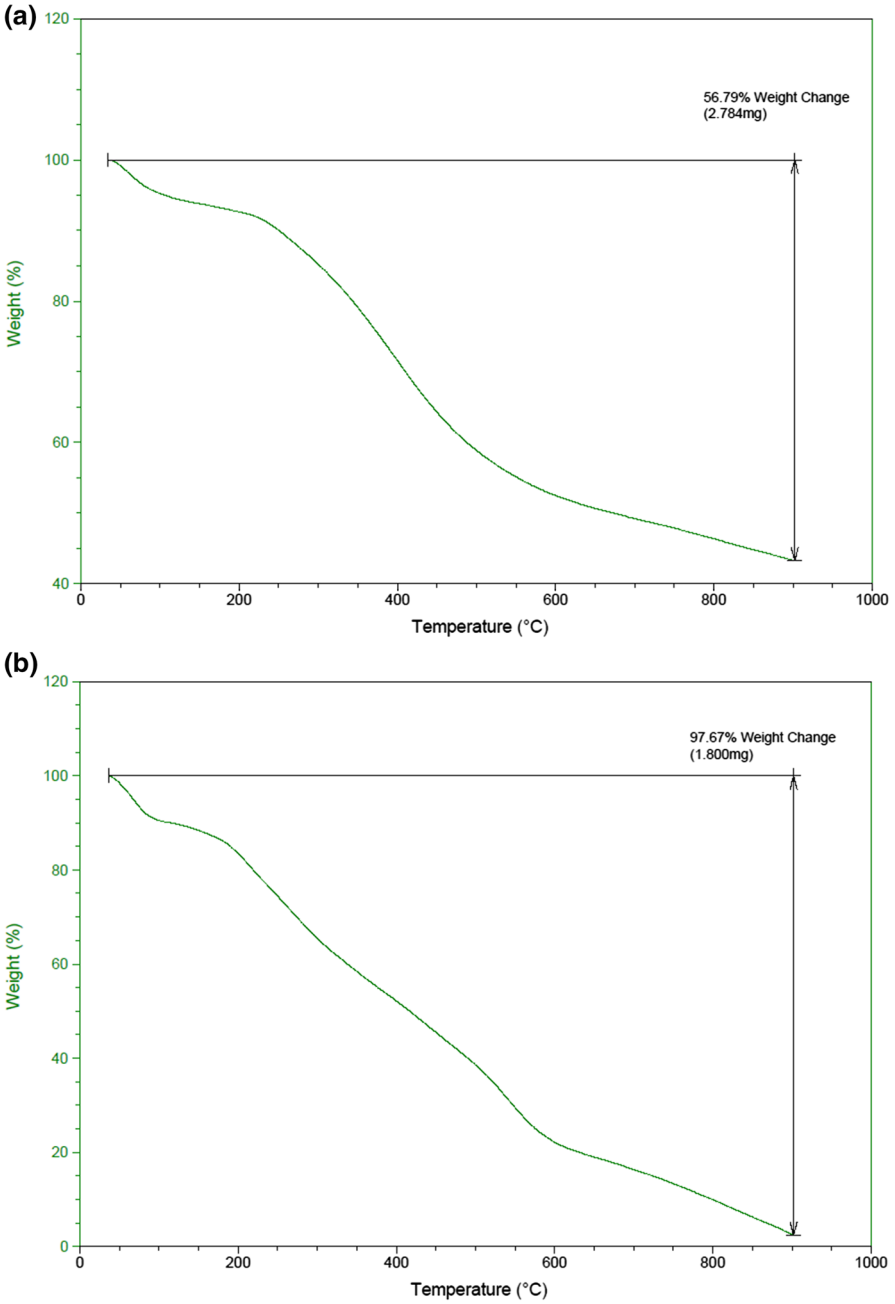

Fig. 5 **a** TGA analysis of RH-SiO_2PrCl. **b** TGA analysis of RH-SiO_2PrANSA

Table 1 Elemental analysis (CHNS) of the RH-SiO_2PrCl and RH-SiO_2PrANSA

Sample	C (%)	H (%)	N (%)	S (%)
RH-SiO_2PrCl	16.24	5.3	–	–
RH-SiO_2PrANSA	29.41	7.3	3.5	4.6

and 4.65%, respectively. The high percentage of these elements is due to the association of RH-SiO_2PrANSA with 1-Amin2-naphthol4-sulfonic acid.

Scanning electron microscopy—energy dispersive X-ray (SEM/EDX)

FESEM micrographs of RH-SiO_2PrCl are shown in Fig. 6. The image indicates a heterogeneous porous structure where several particles gather loosely on the

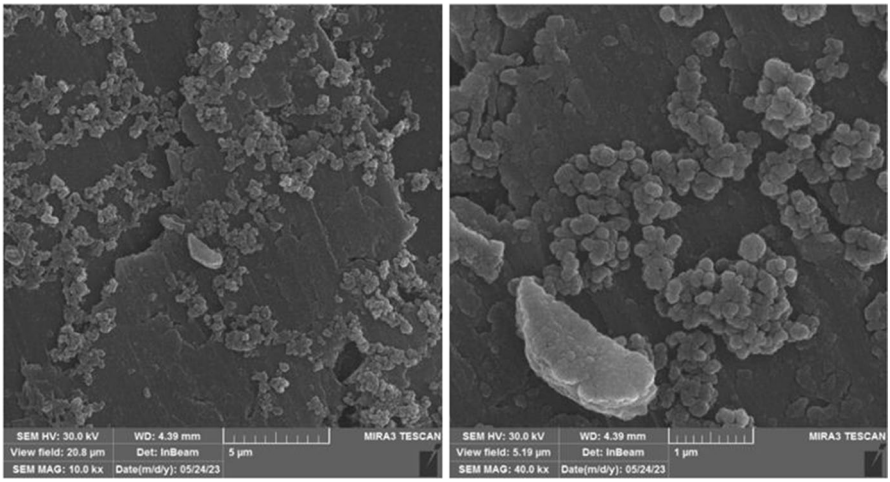

Fig. 6 FESEM analysis of RH-SiO_2PrCl

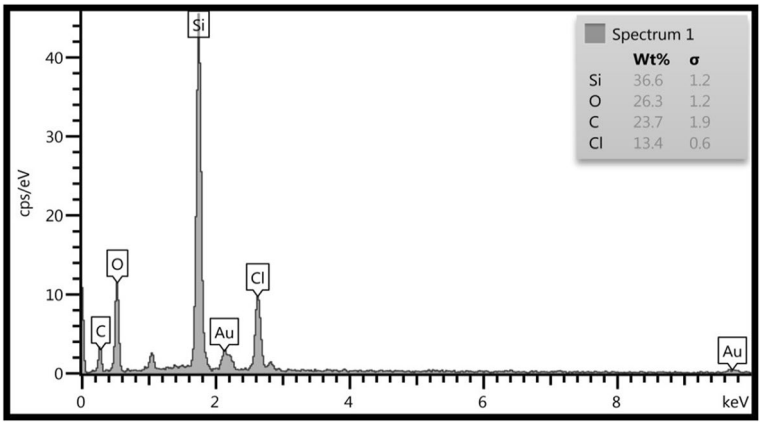

Fig.7 EDX analysis of RH-SiO_2PrCl

sample's surface to form many agglomerates as a result of the functionalized silica by a silylating agent [37]. The EDX spectrum of RH-SiO_2PrCl is shown in Fig. 7. The spectrum analysis revealed that the compounds contained carbon, chloride, oxygen and silicon elements in a compound.

Figure 8 shows microscopic images from FESEM of the RH-SiO_2PrANSA catalyst, where a large gathering of particles appears on the surfaces of the catalyst to form gaps similar to channels and grooves. These gaps facilitate the diffusion of the formed particles on the sample's surface [38]. Figure 9 shows the EDX of RH-SiO_2PrANS. EDX spectrum showed peak density of oxygen 34.80%, carbon. 40.83%, silica 6.01% and nitrogen 18.12%. The synthesized components of this catalyst indicate that the proportion of nitrogen and carbon has increased

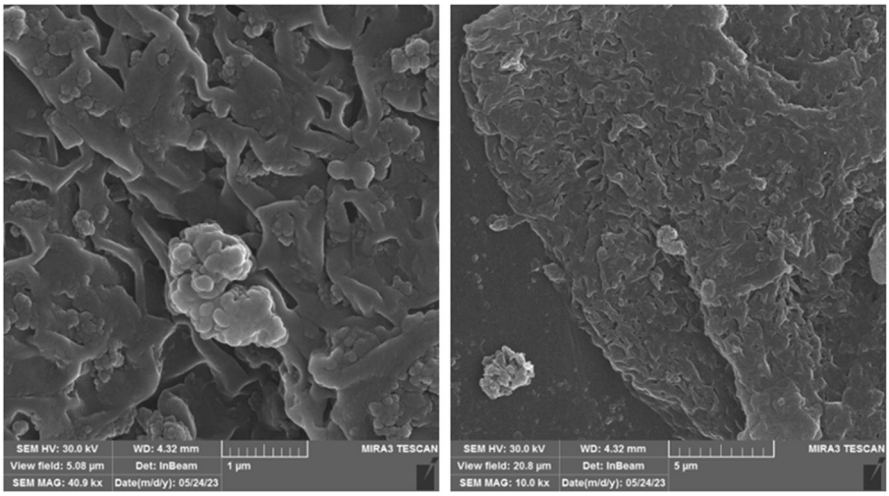

Fig.8 FESEM analysis of RH-SiO_2PrANSA

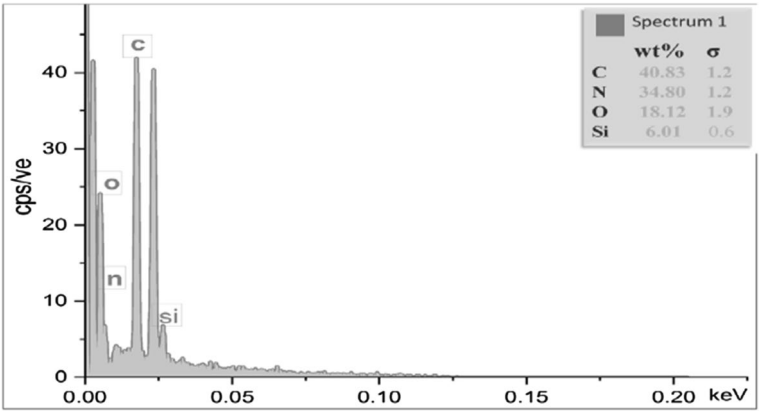

Fig.9 EDX analysis of RH-SiO_2PrANSA

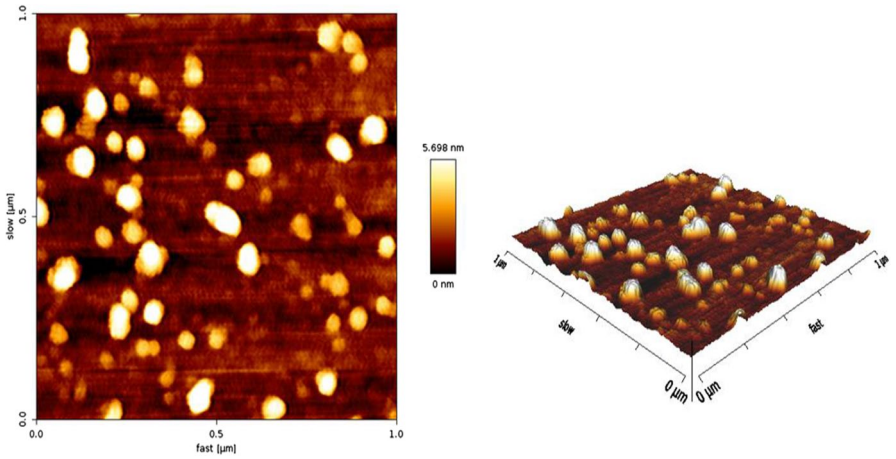

Fig. 10 AFM 2D (in left) and 3D (in right) micrographs of RH-SiO_2PrCl

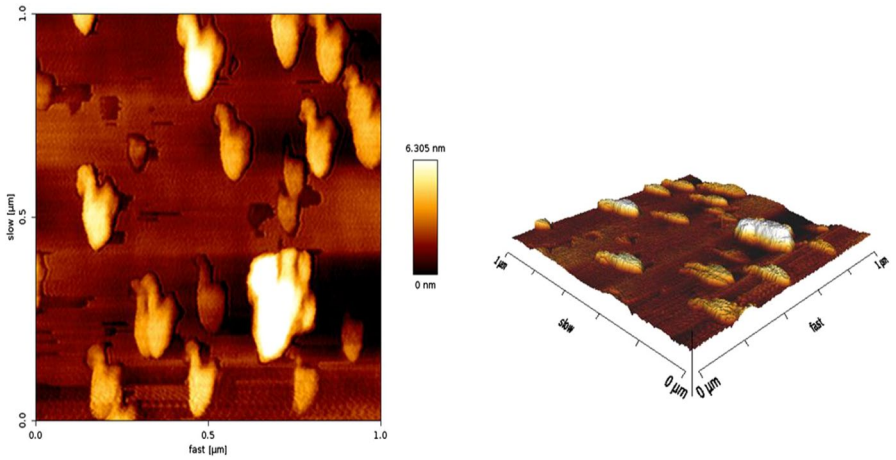

Fig. 11 AFM 2D (in left) and 3D (in right) micrographs of RH-SiO_2PrANSA

compared to the previous catalyst, due to the treatment of this catalyst with 1-Amin-2-naphthol-4-sulphonic acid.

Atomic force microscopy (AFM)

Atomic force microscopy (AFM) images of RH-SiO_2PrCl and RH-SiO_2PrANSA are shown in Figs. 10 and 11, respectively. The structures appear to be pyramidal, and the arrangements of the pores are irregular; the hierarchical structure for RH-SiO_2PrANSA is more compact than for the compound RH-SiO_2PrCl [39]. The average roughness coefficient (Ra) is 1.433 nm, and the root square

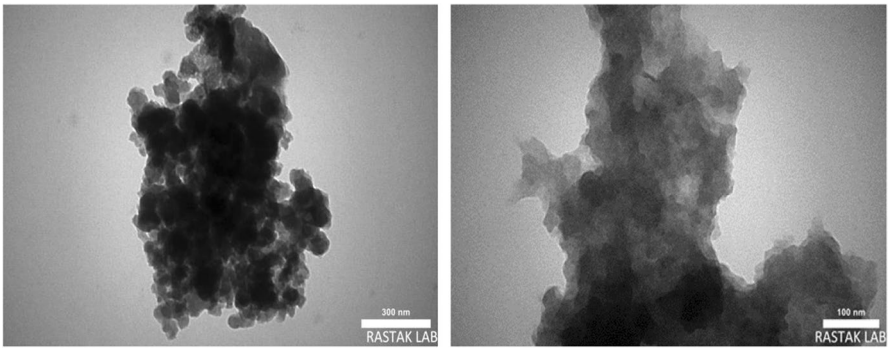

Fig. 12 TEM images of RH-SiO_2PrCl

roughness (Rrms) is 934 pm for the catalyst RH-SiO2PrANSA, which is greater than the roughness coefficient and root square roughness for RH-SiO_2PrCl, 1.295 nm and 845 pm, respectively. This change may be attributed to successfully modifying the surface of the RH-SiO_2PrCl by 1-amin-2-naphthol-4-sulphonic acid.

Transmission electron microscopy (TEM)

The TEM results are shown in the micrographs of the RH-SiO_2PrCl composite composed of amorphous silica in Fig. 12. It can be observed that the pore particles were well distributed with interparticle aggregates. The estimated pore diameter measured is about 4 nm. This result is in agreement with what was obtained from the BET analysis. Figure 13 shows the images of TEM for the RH-SiO_2PrANSA catalyst; the distribution of the pores particles is slightly more dispersed than those of the RH-SiO_2PrCl. As a result of treating this catalyst with 1-amino-2-naphthol-4-sulfonic

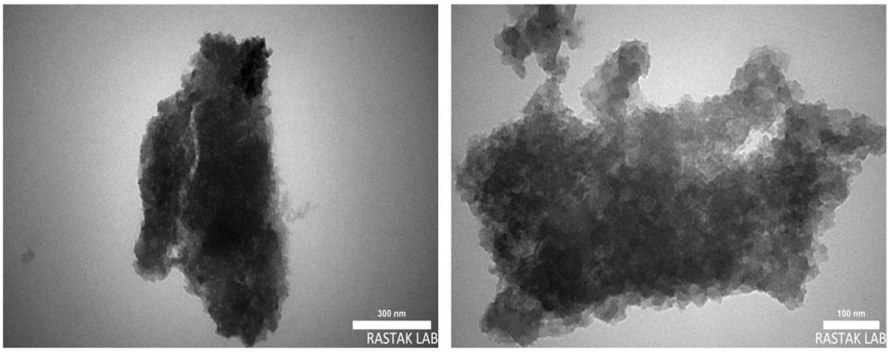

Fig. 13 TEM images of RH-SiO_2PrANSA

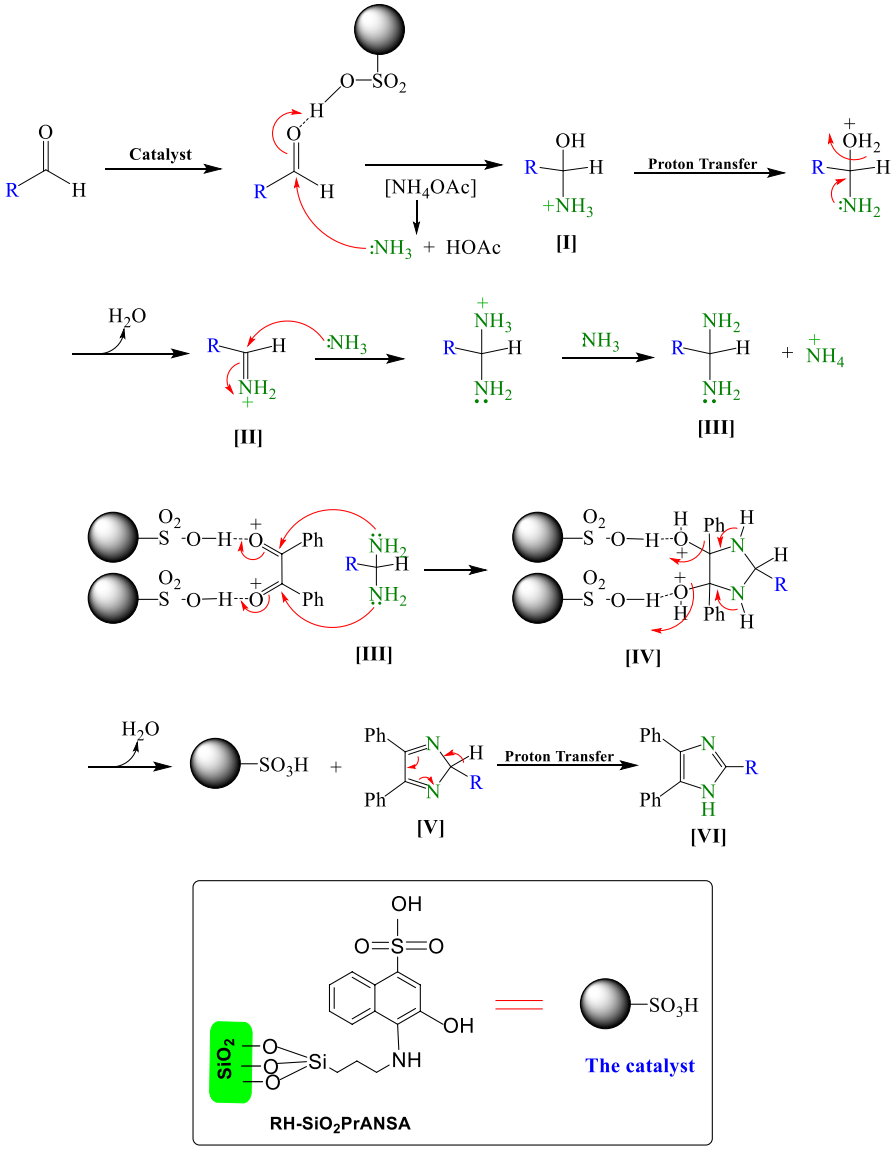

Scheme 3 The possible mechanism of the synthesis of 2,4,5-trisubstituted imidazole derivatives over RH-SiO_2PrANSA

acid, the estimated pore diameter measured was approximately 5 nm. This result agrees with that obtained from the BET analysis, which gives the impression that the RH-SiO_2PrANSA is a mesoporous material.

Characterization of 2,4,5-trisubstituted imidazole derivatives

This research reported an innovative and effective synthetic process for producing 2,4,5-trisubstituted imidazole derivatives from various aldehydes, ammonium acetate, and benzil with RH-SiO_2PrANSA as a catalyst. The synthesis of imidazole derivatives is shown in Scheme 2. The FTIR spectra of all derivatives (**4a-f**) showed two influential bands, one at around 3300 cm^{-1} due to N–H stretching and the other near 1600 cm^{-1} attributed to C=N stretching, while the NMR spectra exhibited a peak of about 12 ppm for the N–H of the ring of imidazole. Moreover, one compound peaked at 2.97 ppm for C–H of the aliphatic group, and two appeared to peak at 9.56 and 9.70 ppm due to O–H of hydroxyl groups. The possible mechanism for forming 2,4,5-trisubstituted imidazole derivatives is suggested in Scheme 3.

The optimization of reaction-conditions

The benzaldehyde, ammonium acetate, and benzil reaction **(4a)** was selected as a model reaction to investigate the most favourable reaction conditions (Scheme 2). The investigation examined several solvents (H_2O, methanol, ethanol, acetonitrile, and THF) screened (Table 1) and molar ratios for the reaction, with the outcomes consolidated in Tables 2 and 3, correspondingly. The most significant percentage yield was attained when ethanol was used as the solvent, as indicated in Table 1, entry 3. This could be due to the good solubility of the catalyst in ethanol. According to the molar ratio analysis, it was determined that the optimal and most appropriate choice for the reaction was a ratio of 1:1:5, as indicated in Table 3, entry 5. Furthermore, the experimental procedure for the model reaction (**4a**) involved utilising different quantities of the catalyst, as shown in Table 4, entry 4, which was demonstrated to improve outcomes by using 0.08 g of the catalyst. After optimising the reaction conditions, a set of 2,4,5-triphenyl imidazole derivatives (4a–f) was synthesized. The catalyst's efficiency with various catalysts by other reported procedures for synthesising 2,4,5-triphenyl imidazole was compared [24, 40]. The best yield was obtained with RH-SiO2PrANSA, as shown in Table 5, entry 3.

Table 2 Effect solvent on the synthesis of 2,4,5-triphenyl imidazole (**4a**)

Entry	Solvent	Yield %
1	H_2O	72
2	Methanol	20
3	Ethanol	97
4	CH_3CN	58
5	THF	40

Table 3 Effect of mole ratio on the synthesis of 2,4,5-triphenylimidazole (**4a**)

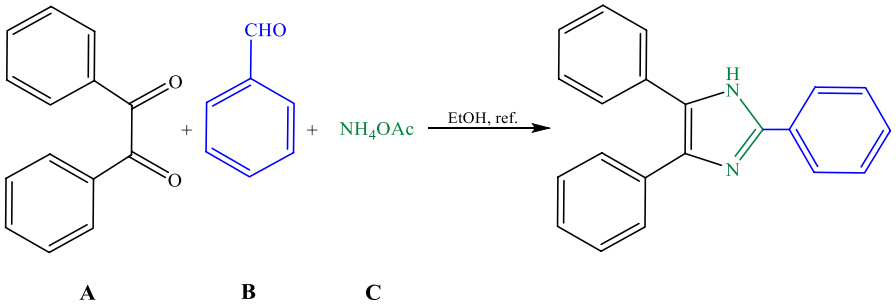

A **B** **C**

Entry	Mole ratio (A:B:C)	Yield %
1	1:1:1	32
2	1:1:2	51
3	1:1:3	69
4	1:1:4	84
5	1:1:5	88

Table 4 Effect of catalyst concentration on the synthesis of 2,4,5-triphenylimidazole (**4a**)

Entry	Catalyst	Yield (%)
1	0.01	64
2	0.02	77
3	0.04	87
4	0.08	95
5	0.16	74

Table 5 Comparisons of some other reported procedures with the present study for the synthesis of 2,4,5-triphenylimidazole (**4a**)

Entry	Catalyst	Reaction conditions	Yield %	Refs.
1	H_2SO_4	Reflux	73	[26]
2	CuI	Reflux	85	[40]
3	RH-SiO_2PrANSA	Reflux	95	This study

Catalyst reusability

A feature of utilizing the novel catalyst, RH-SiO_2PrANSA, is that it is used again, rendering it both ecologically sustainable and cost-effective. A typical response was selected and examined using identically enhanced circumstances to investigate the potential for catalyst reusability. Following the completion of

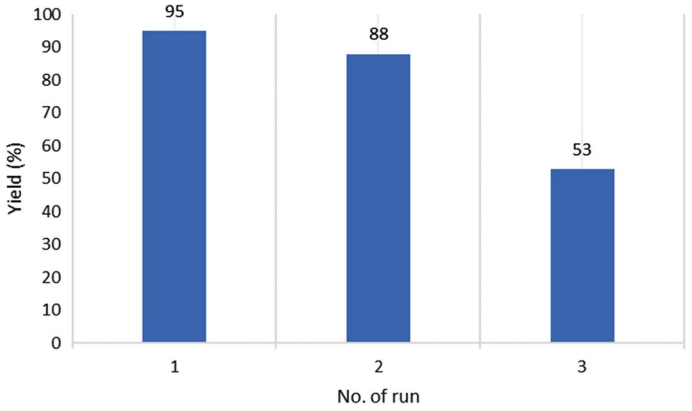

Fig. 14 Reusability of the catalyst

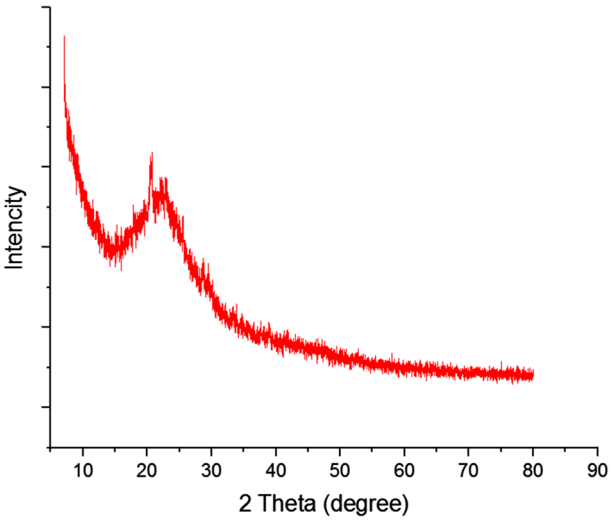

Fig. 15 XRD analysis at high angl of recovered RH-SiO_2PrANSA

the interaction, the catalyst was readily separated by using the reaction combination of a straightforward filtration process and subsequently washed with dichloromethane. The retrieved catalyst underwent a drying process and was put through three more testing times (Fig. 14). Also, from Fig. 14, it is noted that there is a decrease in the effectiveness of the catalyst in the third cycle. The main reason for the decrease in catalytic activity is not clear, but may be related to catalyst toxicity as a result of precipitate organic and inorganic molecules on it. In addition, as shown the XRD spectrum and SEM images (Figs. 15 and

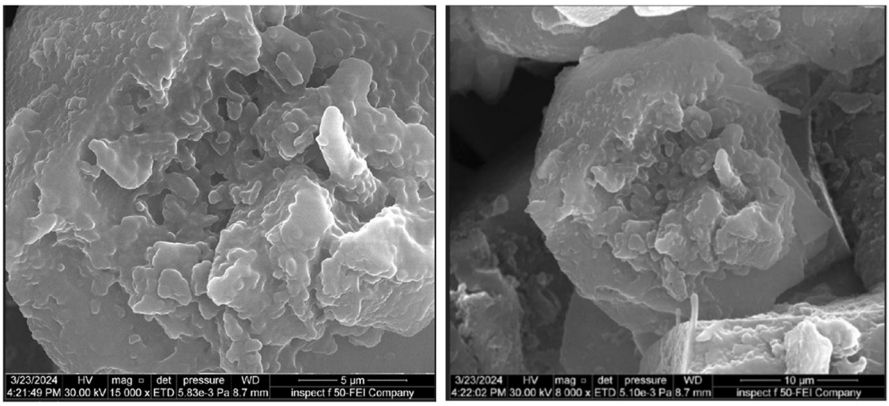

Fig. 16 FESEM analysis of recoverd RH-SiO_2PrANSA

16,respectively) of the recovered catalyst did not change significantly compared to those obtained for the fresh catalysts, indicating excellent structural stability of the solid acid catalyst under reaction conditions.

Conclusion

Based on some physical measurements, such as infrared spectra, elemental analysis, and ED-X, we concluded that the 1-Amin-2-naphthol-4-sulfonic acid had been successfully immobilized onto the surface of functional silica RH-SiO_2PrCl. BET measurements showed the immobilization of a large molecule of the 1-Amin-2-naphthol-4-sulfonic acid on the silica surface, resulting in a significant decrease in the particular surface area for all RH-SiO_2PrCl. The catalyst RH-SiO_2PrANSA, as an efficient and environmentally friendly catalyst, was synthesized and used to prepare imidazole derivatives. The catalyst is recovered for up to three uses without loss of activity. The new methodology gives good yields with simple work-up, mild conditions, and accessible synthesis of catalysts.

Supplementary Information The online version contains supplementary material available at https://doi.org/10.1007/s11164-024-05281-x.

Acknowledgements The authors of the current research paper would like to thank Kerbala University, College of Science, Department of Chemistry for financial support.

Author contributions Noor Abbas Alshook: Performed the experiments and contributed to the manuscript. Hayder Hamied Mihsen: The study's supervisor conceived the ideas, interpreted the physical characterization, and wrote the manuscript. Haitham Dalol Hanoon, Co-supervisor of the study, contributed to writing the manuscript and explained the catalytic process of RH-SiO_2PrANSA in preparing 2,4,5-trisubstituted imidazole derivatives. All authors who have consented to publishing the final draft have seen it.

Funding This project did not receive any funding.

Declarations

Conflict of interests The authors affirm that they do not have any competing interests. It does not require ethics approval.

Data availability The text contains the necessary information and materials.

Consent of participation We now agree to take part.

Consent of publication Each author agrees to the publication.

References

1. I. Oluseun Adejumo, O. Adebukola Adebiyi, in *Strateg. Sustain. Solid Waste Manag.* (IntechOpen, New York, 2021).
2. N. Phonphuak, P. Chindaprasirt, in *Eco-Efficient Mason. Bricks Blocks Des. Prop. Durab.* (Elsevier, Amsterdam, 2015), pp. 103–127.
3. R. Siddique, P. Cachim, *Waste and Supplementary Cementitious Materials in Concrete* (Elsevier, Amsterdam, 2018).
4. S.K. Abbas, Z.M. Hassan, H.H. Mihsen, M.T. Eesa, D.H. Attol, SILICON **12**, 1103 (2020)
5. S. Abualnoun Ajeel, K. A. Sukkar, N. K. Zedin, IOP Conf. Ser. Mater. Sci. Eng. **881**, 012096 (2020).
6. W. Xie, F. Wan, Chem. Eng. J. **365**, 40 (2019)
7. W. Xie, Y. Han, H. Wang, Renew. Energy **125**, 675 (2018)
8. W. Xie, H. Wang, Renew. Energy **145**, 1709 (2020)
9. W. Xie, C. Gao, J. Li, Renew. Energy **168**, 927 (2021)
10. W. Xie, H. Wang, Fuel **283**, 118893 (2021)
11. H. Hattori, Y. Ono, in *Solid Acid Catalysis: From Fundamentals to Applications* (CRC Press, Boca Raton, 2014).
12. H.S. Sobh, H.H. Mihsen, Baghdad Sci. J. **16**, 0886 (2019)
13. N.S. Ahmed, H.D. Hanoon, Res. Chem. Intermed. **47**, 4083 (2021)
14. L.A. Aronica, G. Albano, Catalysts **12**, 68 (2022)
15. N. Kaur, *Raney Nickel-Assisted Synthesis of Heterocycles* (Elsevier, Amsterdam, 2022).
16. F. Adam, K.M. Hello, T.H. Ali, Appl. Catal. A Gen. **399**, 42 (2011)
17. H. Hosseinzadeh, K. Rad-Moghadam, M. Mehrdad, S. Rouhi, Sci. Rep. **14**, 666 (2024)
18. S. Hosseini, A.R. Kiasat, A. Farhadi, Polycycl. Aromat. Compd. **41**, 761 (2021)
19. S. Sangwan, R. Singh, S. Gulati, S. Rana, J. Punia, K. Malik, Curr. Res. Green Sustain. Chem. **5**, 100250 (2022)
20. H.T. Nguyen, P.N. Nguyen, T. Van Le, T.H. Nguyen, L.D. Nguyen, P.H. Tran, RSC Adv. **13**, 28623 (2023)
21. G. Patel, D.K. Dewangan, N. Bhakat, S. Banerjee, Curr. Res. Green Sustain. Chem. **4**, 100175 (2021)
22. H.V. Tolomeu, C.A.M. Fraga, Molecules **28**, 838 (2023)
23. H.H. Ali, K.A. Hussein, H.H. Mihsen, SILICON **15**, 5735 (2023)
24. H.D. Hanoon, E. Kowsari, M. Abdouss, M.H. Ghasemi, H. Zandi, Res. Chem. Intermed. **43**, 4023 (2017)
25. D.A. Hilal, H.D. Hanoon, Res. Chem. Intermed. **46**, 1521 (2020)
26. F. Adam, H. Osman, K.M. Hello, J. Colloid Interface Sci. **331**, 143 (2009)
27. F. Adam, K. Kandasamy, S. Balakrishnan, J. Colloid Interface Sci. **304**, 137 (2006)
28. H. H. Mihsen, S. K. Abass, M. T. Abed AL-Alhasan, Z. M. Hassan, A. K. Abass, Iraqi J. Sci. **61**, 2762 (2020).
29. H.H. Mihsen, S.Y. Rfaish, S.K. Abass, H.S. Sobh, J. Glob. Pharma Technol. **10**, 590 (2018)
30. N.K. Renuka, A.K. Praveen, K. Anas, Mater. Lett. **109**, 70 (2013)
31. A.D. Mohsin, H.H. Mihsen, J. Inorg. Organomet. Polym. Mater. **30**, 2172 (2020)

32. T. Das, A. Roy, H. Uyama, P. Roy, M. Nandi, Dalt. Trans. **46**, 7317 (2017)
33. M. Thommes, R. Köhn, M. Fröba, Appl. Surf. Sci. **196**, 239 (2002)
34. N. Permatasari, T. N. Sucahya, A. B. Dani Nandiyanto, Indones. J. Sci. Technol. **1**, 82 (2016).
35. L. Rout, A. Mohan, A.M. Thomas, C.-S. Ha, Microporous Mesoporous Mater. **291**, 109711 (2020)
36. S. Vaysipour, Z. Rafiee, M. Nasr-Esfahani, Polyhedron **176**, 114294 (2020)
37. M. D. Ahiduzzaman, A. K. M. Sadrul Islam, Springerplus **5**, 1 (2016).
38. H.-Y. Nah, V.G. Parale, H.-N.-R. Jung, K.-Y. Lee, C.-H. Lim, Y.S. Ku, H.-H. Park, J. Sol-Gel Sci. Technol. **85**, 302 (2018)
39. M. Wang, Q. Zeng, B. Zhao, D. He, J. Mater. Chem. A **1**, 11465 (2013)
40. V.D. Kadu, G.A. Mali, S.P. Khadul, G.J. Kothe, RSC Adv. **11**, 21955 (2021)